On the entry and transit of high-density plasma across the polar cap

K. Oksavik,[1] V. L. Barth,[1,2,3] J. Moen,[1,2] and M. Lester[4]

Received 14 June 2010; revised 27 July 2010; accepted 25 August 2010; published 7 December 2010.

[1] Observations are presented from SuperDARN and the EISCAT Svalbard Radar of two intense polar cap patch events on 6 February 2001. The interplanetary magnetic field (IMF) was dominated by a large positive By component, and for both events the electron density exceeded 10^{12} m^{-3} in the *F* region. With SuperDARN we tracked the events all the way across the polar cap, from the dayside Svalbard sector to the nightside Alaska sector. The flow speed was highly dynamic and pulsed, and both patches underwent substantial rotation in the polar cap. On the nightside the leading edge had become the trailing edge. It suggests that the first patch to enter the polar cap on the dayside may not always be the first patch to reach the nightside; plasma might be stagnant in the polar cap or even overtaken. The study also provides evidence that momentum transfer in the dayside polar cap can last significantly longer than 10 min after reconnection, especially for extremely long field lines where IMF By is dominating, i.e., on "old open field lines." Knowledge of the solar wind driver and the coupling processes is therefore extremely important for predicting the motion of a polar cap patch event across the polar cap. Gradients in the plasma flow associated with the rotation of the extreme density may in itself lead to a stronger growth of ionospheric irregularities. These irregularities may continue to grow all the way across the polar cap. The result is more efficient creation of ionospheric irregularities.

Citation: Oksavik, K., V. L. Barth, J. Moen, and M. Lester (2010), On the entry and transit of high-density plasma across the polar cap, *J. Geophys. Res.*, *115*, A12308, doi:10.1029/2010JA015817.

1. Introduction

[2] In the dayside winter polar cap we generally encounter two types of *F* region plasma, low-density background plasma and high-density solar-EUV ionized plasma of subauroral origin. The solar-EUV plasma enters the polar cap from lower latitudes through the cusp inflow region in what is often called a tongue of ionization (TOI) [*Knudsen*, 1974; *Foster et al.*, 2005; *Moen et al.*, 2008a]. *Sato* [1959] was the first to postulate the existence of this TOI, which is regarded as a homogeneous stream of high-density plasma from a dayside sunlit area at lower latitudes that $E \times B$ drifts with streamlines of the anti-sunward convection into and across the polar cap [*Weber et al.*, 1984; *Foster and Doupnik*, 1984; *Buchau et al.*, 1985]. During severe geomagnetic storms this region of high-density plasma is referred to as storm enhanced densities (SED) [*Foster*, 1993], and it extends all the way to middle latitudes where low-latitude solar-EUV plasma in the dusk sector is picked up by enhanced storm-time electric fields [e.g., *Yeh et al.*, 1991] of the Sub-auroral Polarization Stream (SAPS) [*Foster and Burke*, 2002] and transported sunward and toward the high-latitude dayside. Consequently, the latitude of the SED decreases with increasing local time and disturbance level [*Foster et al.*, 2005].

[3] A variety of instruments and techniques have been used to study the occurrence of electron density enhancements in the polar cap, including ionosondes [e.g., *Buchau et al.*, 1983; *Weber et al.*, 1984; *Dandekar and Bullett*, 1999], incoherent scatter radars [e.g., *Lockwood and Carlson*, 1992; *Valladares et al.*, 1994, 1996], HF-radars [e.g., *Rodger et al.*, 1994a, 1994b; *Milan et al.*, 2002, 2005], ionospheric tomography [e.g., *Walker et al.*, 1999; *Pryse*, 2003], and all-sky imaging photometers [e.g., *Lorentzen et al.*, 2004; *Moen et al.*, 2007; *Hosokawa et al.*, 2009a, 2009b, 2009c]. Observations show that the TOI can either be a continuous region, or it can be sliced into a series of discrete substructures [*Moen et al.*, 2006]. Electron density enhancements in the form of isolated islands surrounded by significantly lower density plasma have therefore been named polar cap patches [e.g., *Crowley*, 1996], while the more continuous enhancements of *F* region electron density $n_e \geq 10^{12}$ m^{-3} have been referred to as extreme electron density events [*Moen et al.*, 2008a].

[4] A polar cap patch typically has a density which is 2–20 times larger than the surrounding background electron density [*Buchau et al.*, 1983; *Weber et al.*, 1984; *Crowley et al.*, 2000]. The airglow emission at 630 nm from these

[1]University Centre in Svalbard, Longyearbyen, Norway.
[2]Department of Physics, University of Oslo, Oslo, Norway.
[3]Norwegian Polar Institute, Sverdrup Station, Ny-Ålesund, Norway.
[4]Department of Physics and Astronomy, University of Leicester, Leicester, UK.

0148-0227/10/2010JA015817

patches is also enhanced above the background level. The electron temperature inside a patch is generally low and unstructured, indicating no precipitation of auroral electrons when it is located in the polar cap [*Rodger et al.*, 1994a]. Patches are observed both in winter and summer but are most prominent near the maximum of the sunspot cycle [e.g., *Dandekar*, 2002; *McEwen et al.*, 2004]. They tend to maximize near equinox and around magnetic noon [*Rodger and Graham*, 1996] and have been observed to drift across the central polar cap [*McEwen and Harris*, 1995; *McEwen et al.*, 1995] and exit the polar cap at night [*Lorentzen et al.*, 2004; *Pryse et al.*, 2006; *Moen et al.*, 2007; *Wood et al.*, 2009]. Polar cap patches are sometimes found simultaneously in geomagnetic conjugate regions as well [*Rodger et al.*, 1994b]. Polar cap patches can be 100–1000 km wide in the horizontal direction and are common during moderately disturbed conditions (Kp > 4) [*Weber et al.*, 1984]. The occurrence of polar cap patches also appears to be highly dependent on the orientation and the strength of the interplanetary magnetic field (IMF) [*McEwen and Harris*, 1996; *Hosokawa et al.*, 2006; *Moen et al.*, 2008a]. Traditionally, the polar cap has been thought to be dominated by Sun-aligned arc structures for positive IMF Bz, and polar cap patches for negative IMF Bz [*Crowley*, 1996]. Most reports of polar cap patches are for negative IMF Bz conditions [e.g., *Buchau et al.*, 1983; *Rodger et al.*, 1994a; *McEwen and Harris*, 1996], but *Oksavik et al.* [2006a] reported a special case where a patch formed inside a northward IMF lobe cell due to an extended period of local particle precipitation poleward of the dayside open/closed boundary (OCB), and *Wood et al.* [2008] observed plasma of dayside origin in the midnight sector during northward IMF.

[5] Patches are believed to move across the polar cap with the general convection at typical speeds of 300–1000 m/s to become a blob in the sunward return flow on the nightside [*Weber et al.*, 1984]. These blobs are divided into three types; subauroral blobs, boundary blobs, and auroral blobs. Boundary blobs are found near the equatorward auroral boundary [*Crowley*, 1996]. Auroral blobs are probably formed by particle precipitation inside the auroral oval, while subauroral blobs are formed by transport effects.

[6] On their way across the polar cap, patches are known to have significant negative effects on various radar and radio systems, including ground-to-satellite links and other navigation and communication systems [e.g., *Basu et al.*, 1990, 1998]. Extensive research has therefore been made to predict the occurrence of these patches and to develop space weather forecasts [*Schunk and Sojka*, 1996; *Basu et al.*, 2002]. There have also been several studies involving two-dimensional (2-D) trajectory analysis codes [e.g., *Crowley et al.*, 2000]. In a recent study *Bust and Crowley* [2007] combined the techniques of 3-D ionospheric assimilation and 2-D trajectory codes. But neither technique can provide complete information on the transport of plasma patches; the 2-D trajectory code does not contain information about electron densities, and the 3-D ionospheric assimilation code lacks information about the convection. As pointed out by *Crowley et al.* [2000], the polar cap has traditionally been an area of poor data coverage, making it especially difficult to study the detailed motion and evolution of polar cap patches.

[7] In this paper we will try to address this complex issue by presenting actual measurements of polar cap patches from the EISCAT and SuperDARN radars during an interval of exceptional wide data coverage. The EISCAT Svalbard Radar is used to identify extreme electron densities in the dayside polar cap. By extreme electron densities we mean electron densities exceeding 10^{12} m^{-3} in the *F* region. Using simultaneous SuperDARN measurements of enhanced backscatter power and plasma flow, we follow the motion of the patches all the way across the polar cap (from the dayside Svalbard sector to the nightside Alaska sector).

2. Data Presentation

[8] In February 2001 and October 2002 the EISCAT Svalbard Radar (ESR) performed a series of long-duration runs during a period of high geomagnetic activity. The data set is composed of 20 and 27 days of continuous observations, respectively. *Barth* [2009] surveyed this entire data set and found 06 February 2001 to be especially interesting. On that day there were two extreme density events over the ESR, and SuperDARN had wide and extensive coverage across the entire Northern Hemisphere polar cap. In this paper we study those events in much greater detail, with the aim of shedding light on how the extreme density events traversed the polar cap.

[9] In Figure 1 we present an overview of the field-aligned ESR data (42 m beam) from 0600 to 1100 UT. Figure 1a shows the maximum electron density in each altitude profile. A horizontal line indicates our extreme density limit of 10^{12} m^{-3}. In Figure 1a, there are two events within 1.5 h of magnetic noon (0900 UT) which exceed that limit (0723–0740 UT and 0800–0819 UT, indicated with vertical guide lines and numbers 1 and 2). The duration of these events is 17 and 19 min, respectively. In Figures 1b to 1e the altitude profiles of the electron density (Ne), the electron and ion temperature (Te, Ti), and the line-of-sight ion velocity (Vi) versus time are shown in color scale for the height range 100–800 km. In Figure 1b the height of the maximum electron density is plotted with black dots overlaid on the electron density profiles. Around 0630–0800 UT the electron density peaks between 400 and 500 km altitude. For the remainder of the interval the electron density peaks between 300 and 400 km altitude. The electron temperature in Figure 1c is mostly high (suggesting electron heating), except during the two extreme density events indicated with the vertical guidelines. Low electron temperature is an indicator of no local electron particle precipitation, i.e., there is no heating due to precipitation. The ion temperature in Figure 1d is high before 0715 UT and low until 0815 UT, after which there is a series of transient enhancements. The line-of-sight ion velocity in panel e is characterized by a series of ion upflow and downflow events. Before 0715 UT there is both strong upflow and enhanced electron temperature, which is characteristic of the dayside cusp region. *Moen et al.* [2004] have also related this type of ion upflow to cusp aurora. During event 1, and between events 1 and 2, there is a series of transitions between upflow and downflow. Event 2 is primarily associated with downflow, while the remainder of the day is characterized by a series of upflow events. This type of ion upflow is very commonly measured by the ESR between 0600 and 1200 UT (0900–1500 MLT), and ion downflow is present only when the geomagnetic activity is high, i.e., when the auroral oval has

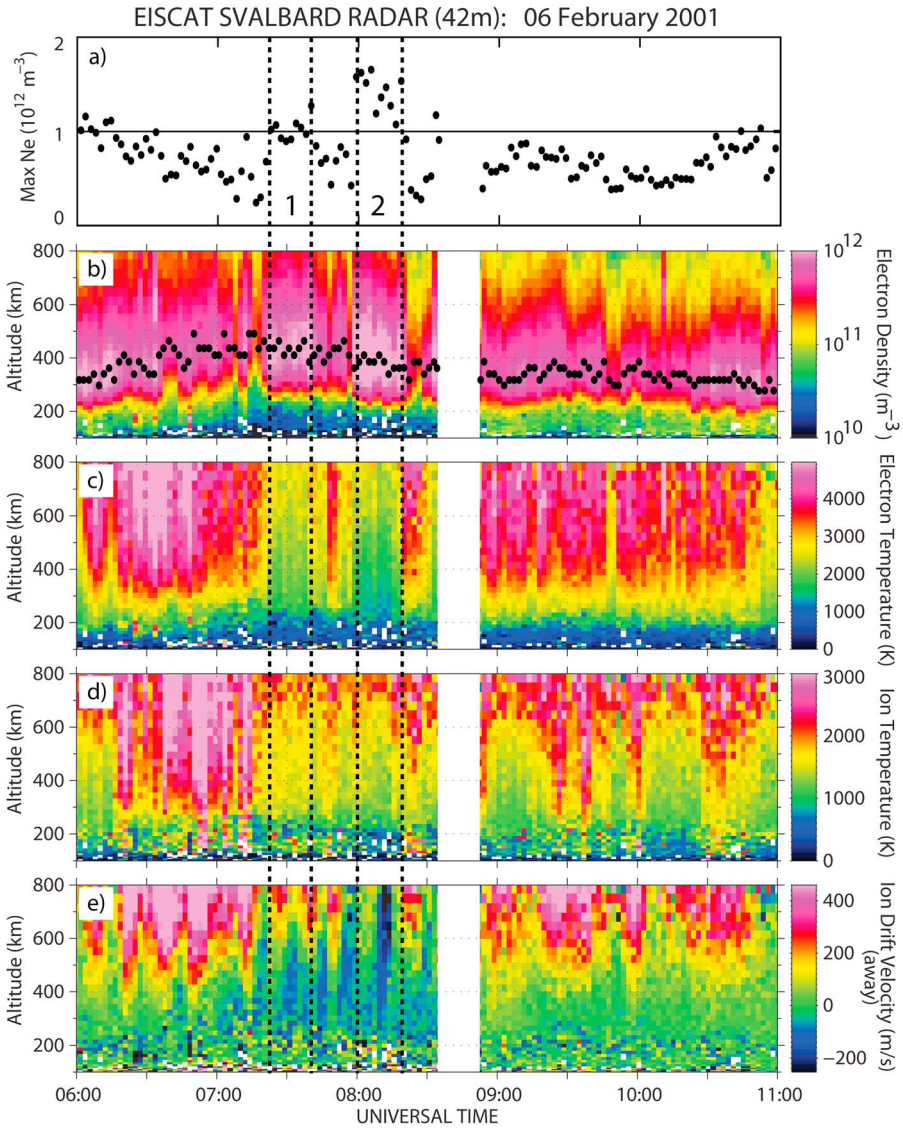

Figure 1. Measurements from the EISCAT Svalbard Radar field-aligned antenna from 0600 to 1100 UT on 06 February 2001. (a) Maximum electron density in the *F* region ionosphere. Two intervals of extreme electron densities $>10^{12}$ m^{-3} are indicated with numbers 1 and 2. (b) Electron density profiles in color and the peak of the *F* region with black dots. Profiles of (c) electron temperature, (d) ion temperature, and (e) vertical ion velocity.

expanded equatorward and the ESR is situated in the polar cap [e.g., *Ogawa et al.*, 2009]. These authors also found ion upflow to be frequently accompanied by ion and electron heating, with increasing occurrence frequency of ion upflow for increasing IMF By strength which is, as we shall see, similar to the situation for the day we study here.

[10] In Figure 2 we present an overview of ACE interplanetary magnetic field (IMF) data and SuperDARN observations. ACE was located at $[X, Y, Z]_{GSM} = [239.5, -26.4, 19.3]_{Re}$. Unfortunately, ACE was only able to provide magnetic field data, but SOHO was located nearby and it detected an average solar wind speed during the interval of 390 ± 6 km/s at $[X, Y, Z]_{GSM} = [194.1, 34.8, 22.9]_{Re}$. In addition WIND measured an average solar wind speed of 393 ± 16 km/s at $[X, Y, Z]_{GSM} = [-38.3, 163.6, 17.2]_{Re}$, suggesting that the solar wind speed was fairly uniform and stable over a wide area around ACE. If we simply divide the distance by the solar wind velocity, an average solar wind speed of 390 km/s gives a solar wind propagation delay of 65 min from ACE to the Earth. A more sophisticated treatment [e.g., *Lockwood et al.*, 1989] gives the same result. So in an effort to ease the comparison with other data, in Figure 2 we have time shifted Figures 2a to 2c by 65 min. Figures 2a–2c show the IMF Bx, By, and Bz components from ACE, respectively, and the time of the two extreme electron density events from Figure 1 are indicated with vertical guide lines. During both events Bx was strongly negative and By was strongly positive. Bz was strongly negative during the first event and had a northward transient during the second event.

[11] Figure 2d shows the SuperDARN polar cap potential. Just before event 1 it exceeded 110 kV, and just before

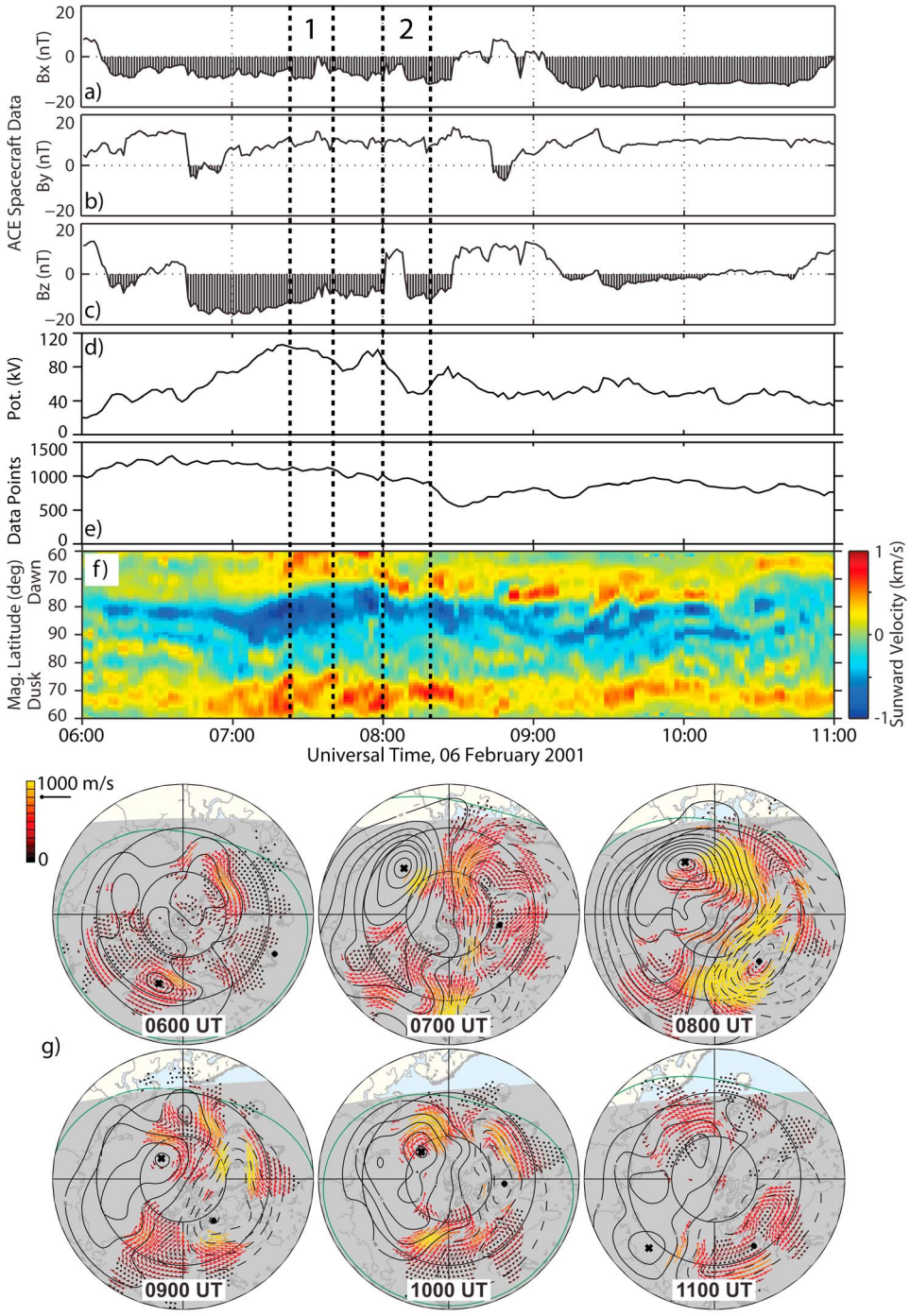

Figure 2. Measurements from the ACE spacecraft and SuperDARN from 0600 to 1100 UT on 6 February 2001. The dashed vertical guide lines indicate the times of the two extreme electron density events in Figure 1. Interplanetary magnetic field (a) Bx, (b) By, and (c) Bz components in GSM coordinates. The ACE data has been time shifted by 65 min, to account for the solar wind propagation delay from the spacecraft location to the dayside magnetopause. (d) Polar cap potential and (e) the number of data points in the SuperDARN map-potential model for the Northern Hemisphere. (f) Sunward (in red colors) and antisunward (in blue colors) SuperDARN plasma flow in a dawn-dusk meridional cut across the polar cap at 0600 and 1800 MLT. (g) Six frames of the SuperDARN convection pattern (at 0600, 0700, 0800, 0900, 1000, and 1100 UT). At that time the data coverage was extensive across the day, dawn, and night ionosphere. The boundary between the shaded and unshaded areas represents the approximate location of the solar terminator at ground level.

event 2 it exceeded 100 kV. We notice that there were transient enhancements in the polar cap potential just before both events, which is needed to bring dense plasma from lower latitudes into the ESR field-of-view (at the time located in the polar cap). Figure 2e shows the number of SuperDARN data points in the Northern Hemisphere magnetic grid. For both events it was very high and above 1000 data points, which is close to the maximum coverage obtained in 2001, i.e., well above a more typical coverage of 300–700 data points. The 1000 data points cover a geographical area similar to the size of the entire polar cap poleward of 72° MLAT. Figure 2g presents six frames of the SuperDARN convection pattern (i.e., once per hour from 0600 to 1100 UT). At the start of this interval Svalbard was located around 75° MLAT in the prenoon to noon sector. The SuperDARN coverage was especially great in the time range 0700–0900 UT across the dayside, morningside, and nightside sectors. Conditions were therefore excellent for tracing the two events from the dayside and across the polar cap. Figure 2f shows a cross-section of the convection pattern along the 1800 to 0600 MLT meridian, in order to show temporal variations in the sunward flow (in red color) and antisunward flow (in blue color). In both the dawn and dusk sectors the sunward flow was particularly strong between 60° and 70° MLAT, with several transient enhancements in the sunward flow speed. The antisunward flow across the polar cap (shown in blue color) was particularly strong from 0700 to 0830 UT in the dawn sector. The high flow speed is consistent with IMF Bz being negative, and the flow slows down when IMF Bz later turns positive. The dawn-shift of the flow channel is also consistent with IMF By > 0, i.e., a By > 0 flow pattern. But there is also substantial variation in the dawn-dusk location of the blue antisunward flow channel in the dawn sector. From 0700 to 0800 UT it migrates gradually toward lower latitudes consistent with a general expansion of the polar cap during the extended period of Bz < 0 and By > 0. When Bz turns northward at 0800 UT the flow channel returns toward higher latitudes. There are also several examples of pulses in the antisunward flow, indicating a highly dynamic convection pattern.

[12] SuperDARN convection patterns were created using the technique of *Ruohoniemi and Baker* [1998]. It combines all available SuperDARN data in one hemisphere by (1) median filtering the Doppler velocity data in range, azimuth, and time to remove noise/marginal values; (2) binning the filtered data onto a uniform grid of equal area cells; (3) selecting an equatorward boundary for the convection zone where the electrostatic potential is set to zero; (4) estimating the velocity in regions of poor data coverage using a model pattern based on IMF By and Bz data [*Ruohoniemi and Greenwald*, 1996]; and (5) solving Laplace's equation to obtain a solution for the ionospheric electrostatic potential as a weighted least squares fit to a spherical harmonic expansion of Legendre functions. In the fitting procedure, model estimates are weighted lower than gridded data to ensure that the model constrains the solution in areas of poor coverage without disturbing the results near the velocity measurements. The result is an array of flow vectors across the entire polar cap at 2-min cadence and with a grid resolution of 1° MLAT and 2° MLON. These data were then used to trace the extreme densities forward and backward in time in the following way. Using event 1 as an example, a new test particle is injected every minute from 0723 to 0740 UT at the ESR location (i.e., 75.37° MLAT and 113.94° MLON). The MLT of each data point was determined, and the closest flow vector was used to trace the test particle toward the next minute boundary. This new location was then used as the next starting point, and the process was repeated. In the examples to be presented below each test particle will be traced 2 h backward and 2 h forward in time. It should be noted that in the area covered by the grid there is at least one flow vector within 0–115 km range (i.e., maximum 1° MLAT away). We also tried to skip the closest vector and use the next flow vector instead (i.e., to test for uncertainties in flow direction/magnitude introduced by the technique). However, it only led to very tiny differences, so this technique should be more than sufficient to reproduce the large-scale picture and all major trends.

[13] The upper row of Figure 3 presents the tracing results for events 1 and 2, where the paths (backward and forward in time) of plasma parcels passing the ESR beam every minute from 0723 to 0740 UT (event 1) and 0800 to 0819 UT (event 2) can be seen. Color indicates how reliable the tracing is, i.e., the number of unique SuperDARN measurements in a 2-min interval within a 100 km radius. Dark blue color (a value of 0) means that no measurements were available, i.e., only the SuperDARN model was used. Solid black lines in Figure 3a indicate the location of the extreme density plasma every half hour from 0700 to 0930 UT. The time is plotted on the same side of the track as the leading edge (i.e., indicates where the plasma that passed the ESR at 0723 UT is located). The stretching out over the ESR is simply due to the fact that that the density is being added at that location (i.e., the convection takes the density away from the region in roughly the same direction). If we look at the backward tracing (i.e., at 0700 UT), the high-density plasma appears to arrive from a broad region near 70° MLAT (i.e., close to the terminator at the time). We should note that we have not drawn any black lines for 0630, 0600, and 0530 UT, because prior to 0700 UT the flow speeds were so low that the plasma hardly moved. In the particle tracing the test particles can be considered to be similar to pearls on a string, with the leading edge in the prenoon sector and the trailing edge in the postnoon sector. The reason for this east-west alignment is a gradual strengthening of By > 0 at the time; i.e., a transition from a symmetrical two-cell convection pattern to a By > 0 type convection pattern with a crescent shaped morning cell. At 0730 UT the string of high-density plasma is stretched out over the ESR site, moving poleward toward northwest, where the leading and trailing edges follow the same path like pearls sliding along a string. At 0800 UT the motion is primarily antisunward, and the trailing edge has been following the same path as the leading edge. But now the leading edge has started to diverge toward dusk, while trailing edge is following a path closer to dawn. The net effect is a slow clockwise rotation of the entire region of high-density plasma. This effect can be seen even clearer at 0830 UT, where the leading edge has crossed the noon-midnight meridian, and the string of extreme density plasma is starting to slide sideward. This rotation even appears to continue, and at 0930 UT the trailing edge has completely overtaken the leading edge and it has reached the lowest latitude on the nightside. Around 0850–0910 UT this event is expected to transit the northern

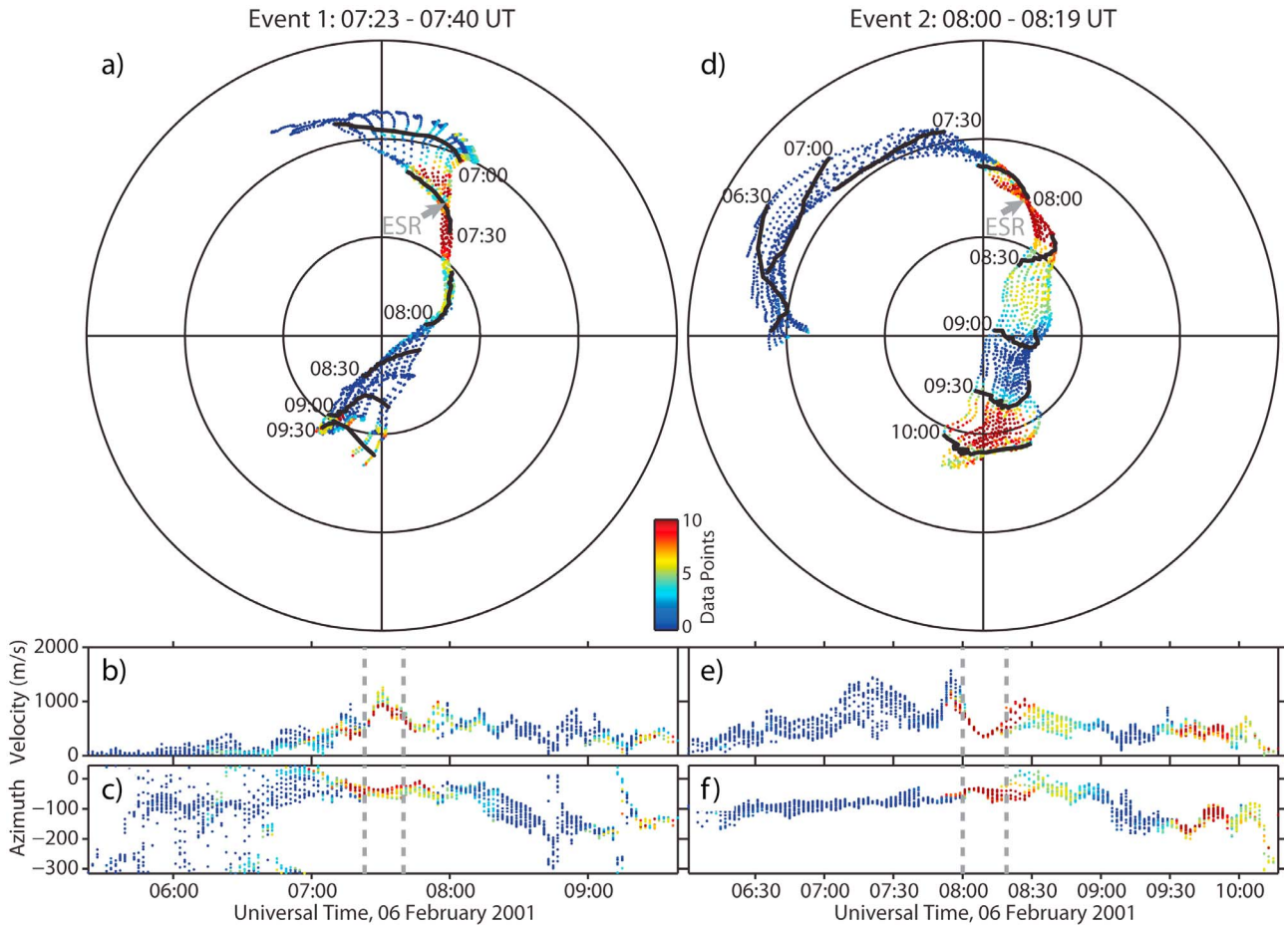

Figure 3. Resulting trajectories across the polar cap based on a particle tracing of events 1 and 2. (a) Event 1, which shows the paths (backward and forward in time) of plasma parcels that passed the ESR beam every minute from 0723 to 0740 UT. (b and c) The corresponding flow speed and flow direction in magnetic azimuth versus time. (d) Event 2, which shows the paths (backward and forward in time) of plasma parcels that passed the ESR beam every minute from 0800 to 0819 UT. (e and f) Corresponding flow speed and flow direction in magnetic azimuth versus time. The vertical guide lines in Figures 3b–3c and Figures 3e–3f indicate the time of events 1 and 2, respectively. Thick black lines in Figures 3a and 3d indicate the location of the high-density plasma every half hour. Color is used in Figures 3a–3f to indicate the number of SuperDARN data points within a 100 km radius; i.e., a higher number equals more reliable tracing and zero indicates that only the SuperDARN model was available (dark blue color).

part of the Kodiak radar field-of-view in the Alaskan sector, but unfortunately the data coverage was poor.

[14] In Figure 3d we show the results for event 2, where the paths (backward and forward in time) of plasma parcels passing the ESR every minute from 0800 to 0819 UT can be seen. The situation is similar to that of event 1, but event 2 starts in a period when By is even more positive, so the extreme density plasma appears to originate even further into the afternoon sector. At 0730 UT the test particles are again aligned like pearls on a string, with the leading edge near noon and the trailing edge far into the afternoon sector. At 0800 UT the leading edge intersects the ESR beam, and both the leading and trailing edges follow the same path, along a straight line toward the northwest. At 0830 UT a dramatic rotation of the high-density plasma has occurred. Now the leading edge is closer to magnetic noon, while the trailing edge is sliding further toward dawn. At the same time the string of extreme density plasma starts to slide sideways in the antisunward direction. This sideways motion continues across the entire polar cap, and at 1000 UT both the leading and trailing edges are aligned along the L-shell, i.e., they arrive in the nightside sector almost simultaneously. Consequently, there has been a transition from a mainly meridional alignment on the dayside to a mainly longitudinal alignment on the nightside, i.e., from 0800 to 1000 UT the entire feature has rotated more than 90° in the clockwise direction relative to the noon-midnight meridian! For later reference we also note that around 0920–0950 UT this feature is expected to transit the northern part of the Kodiak radar field-of-view in the Alaskan sector.

[15] In Figures 3b and 3e we show the actual flow speeds of the high-density plasma versus time, and in Figures 3c and 3f we show the flow direction in magnetic azimuth versus time. Indicated with dashed gray guide lines are the

time intervals when the high-density plasma intersected the ESR beam. The flow speed is highly variable, with a series of flow pulses. For event 1 in Figure 3b there is a small flow pulse just before the plasma reached the ESR location (around 0715 UT); i.e., a burst of reconnection transports the high-density plasma from the subauroral sunlit reservoir and into the polar cap. A second pulse is seen when the high-density plasma is over the ESR (around 0730 UT). A third pulse is seen when the plasma has moved poleward of the ESR (around 0800 UT). For each pulse there is a spread in velocity, meaning that different parts of the high-density plasma are experiencing different flow speeds. At the same time there is also a spread in flow direction, hence indicating a weak rotation of the high-density plasma. From 0800 to 0900 UT this rotation is substantial (there is a wide spread in azimuth directions). At the same time the extreme density plasma is rotating around, and the trailing edge overtakes the leading edge. A similar situation is seen for event 2 in Figure 3e. There is a substantial flow pulse just before 0800 UT which brings the extreme density plasma quickly poleward and into the ESR field-of-view. During a second pulse around 0830 UT there is a strong gradient in the flow speed, the high-density plasma rotates, and the trailing edge overtakes the leading edge.

[16] For event 2 there is extensive data from both Hankasalmi and Kodiak to document the actual rotation of the plasma in the high-latitude dayside polar cap and the subsequent arrival in the nightside sector. In Figures 4a and 4b, two radar scans of backscatter power measurements from the dayside Hankasalmi radar are shown at 0826 and 0839 UT, respectively. Event 2 is encircled with a dashed line, and there is a significant rotation of the area of enhanced backscatter. The spatial extent and the poleward motion are entirely consistent with the particle tracing of Figure 3. From 0826 to 0839 UT the western edge in the prenoon sector is making substantially faster progress in the poleward direction than the eastern edge. This is more clearly shown in Figures 4c and 4d, which are range versus time plots of the Hankasalmi beams 5 and 9. Beam 5 is in the western (prenoon) sector of the field of view, and here the enhanced backscatter and therefore plasma density is drifting poleward at a speed of 566 m/s (indicated with the dashed line). In beam 9, which is in the eastern (noon) sector of the field of view, the poleward speed is only 226 m/s. Consequently, there is a net velocity shear across the high-density region, causing the rotation seen in Figures 4a and 4b.

[17] The high-density plasma was expected to enter the nightside ionosphere around 0920 to 0950 UT, and Figure 4g shows a range versus time plot from beam 2 in the western part of the Kodiak field of view. A dashed line indicates the equatorward progression. The equatorward speed was around 365 m/s and uniform across the entire field of view. Figures 4e and 4f show two individual scans of the Kodiak radar at 0930 and 0940 UT, where the region of extreme density has been encircled with a dashed line. According to the results in Figure 3, at 0930 UT the leading edge of the high-density plasma would have reached to 84° MLAT, while the Kodiak radar has wide backscatter from 80° to 85° MLAT (Figure 4e). Ten minutes later, at 0940 UT, the tracing has reached to 82° MLAT, while the Kodiak radar has wide backscatter from 79° to 83° MLAT (Figure 4f).

[18] A key factor for this comparison is the accuracy of the SuperDARN Doppler velocity measurements. Many attempts at evaluating the accuracy of HF radar Doppler velocity measurements have found a reasonable agreement with other data sets [e.g., *Villain et al.*, 1985; *Ruohoniemi et al.*, 1987; *Baker et al.*, 1990; *Grant et al.*, 1995]. Other studies suggest that SuperDARN velocities at times can be 10–30% smaller than satellite or incoherent scatter measurements [e.g., *Davies et al.*, 1999; *Xu et al.*, 2001; *Drayton et al.*, 2005]. Some of this discrepancy can be due to differences in observation volumes (wider SuperDARN radar beam compared to incoherent scatter radars). *Gillies et al.* [2009] have also suggested that the refraction index in the scattering region could play a role and lead to an underestimation of the Doppler velocity if it is not accounted for.

[19] An interesting exercise is therefore to look at the velocities of the current data set. Using the 0930 UT case in Figure 4e as an example, we can calculate the net traveled distance (from the ESR to Kodiak) and estimate the average flow speed across the polar cap. The original values give a traveled distance of 2300 km in 90 min (i.e., an average speed along the trajectory of 425 m/s). To align the tracing with the middle of the backscatter area, we have to increase the average speed by 9% to 463 m/s (or shortening the transit time across the polar cap by ~10 min). Such a small discrepancy can in principle be accounted for by considering issues like the refraction index in the scattering volume [*Gillies et al.*, 2009]. However, we also need to consider other more critical factors like the uncertainty in the exact location of the Kodiak backscatter (we do not know the exact raypath from the Kodiak radar to the irregularities in the ionosphere). *Yeoman et al.* [2001] have found that the standard algorithm for backscatter ground range location is only accurate to within 114 ± 15 km for 1.5F mode backscatter. Given the uncertainty of the measurements, the arrival of the high-density plasma in the nightside is therefore fully consistent with the findings of the particle tracing in Figure 3. The extensive data set documents that the plasma did experience a net rotation as it traversed the polar cap.

3. Discussion

3.1. Motion and Source of High-Density Plasma

[20] This result has several very interesting consequences; if we observe a polar cap patch on the dayside, we can no longer assume that its leading edge will also be first to enter the nightside ionosphere. If there is a time-varying electric field or strong shears in the plasma flow (e.g., due to a strong IMF By component), the patch may experience substantial rotation on its way across the polar cap. What may start out as a north-south elongated feature on the dayside may turn into an east-west elongated feature on the nightside. In other words, the appearance of a polar cap patch does not have to be preserved as it moves across the polar cap. Under the influence of gradients in the electric field, its geometrical shape may be transformed (stretched, squeezed, curved, etc). Figure 2f also provides some very key information on the flow speed it will experience across the polar cap. For strong IMF By conditions the flow is not uniform along a dawn-dusk slice across the polar cap. For IMF By > 0 the highest

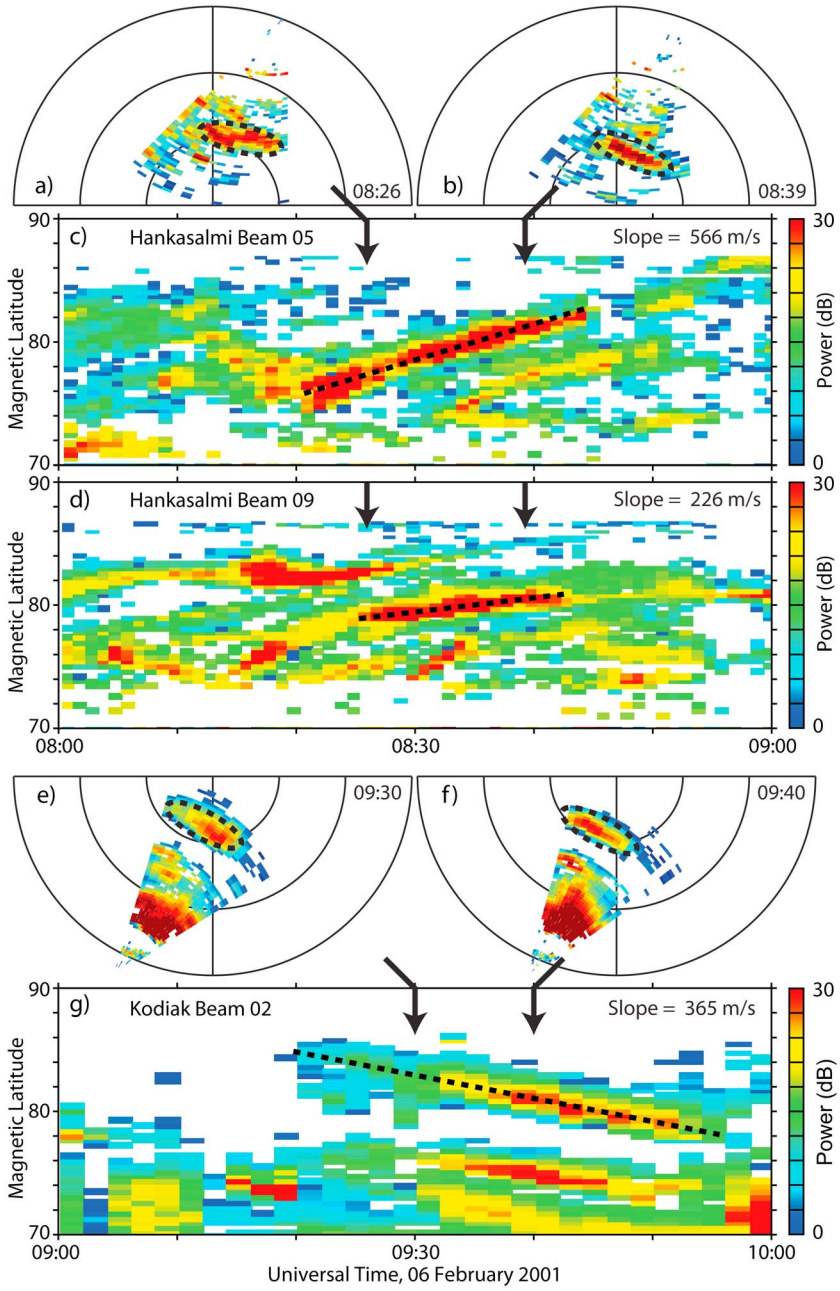

Figure 4. Backscatter power measurements of event 2 from the SuperDARN radars at Hankasalmi (Finland) and Kodiak (Alaska). Two snapshots at (a) 0826 and (b) 0839 UT from Hankasalmi of an area of enhanced backscatter power that rotated in the clockwise direction just north of Svalbard. The event is encircled with a dotted line. The poleward motion in the (c) western (beam 5) and (d) eastern (beam 9) parts of the Hankasalmi field-of-view. The event is indicated with dashed lines, and the slope verifies that the western edge of the event moved poleward at substantially higher speed, i.e., consistent with a clockwise rotation. Two snapshots at (e) 0930 and (f) 0940 UT from Kodiak of an area of enhanced backscatter power. The event is encircled with a dotted line, and it has drifted across the polar cap, but maintained its orientation. (g) Beam 2 of the Kodiak radar, showing a steady equatorward motion of the event once it reached the nightside. A magnetic grid is used in Figures 4a–4b and 4e–4f, with 10° latitude per division, and noon facing up and dawn to the right.

antisunward flow is in a narrow channel just poleward of the open-closed boundary in the dawn sector (indicated with dark blue colors between 80 and 90 MLAT in the dawn sector). Figure 2f also shows that the location of highest drift speed may shift under the influence of a time-varying IMF. So on its way across the polar cap, a patch may experience a highly varying drift speed with time. When the patch is sitting in the middle of the flow channel it will move

quickly, when it is outside the flow channel it will move slowly, and when it is partly inside and partly outside the flow channel it will rotate. For example if there is a change in IMF By (i.e., a sign or amplitude change), this also opens the possibility that the first patch to enter the dayside polar cap may not be the first to leave the polar cap on the nightside. Imagine a patch being launched into the dayside polar cap. Just after launch there is a change in IMF By and the high-speed flow channel changes its orientation so the patch is left in an area of slower plasma flow. If a second patch is launched into the dayside polar cap and it stays in an area of higher antisunward flow speed, it could reach the nightside polar cap before the slower moving patch. Consequently, polar cap patches may experience a broad range of plasma flow conditions on their way across the polar cap. The first patch to enter the dayside polar cap may not be the first to leave the nightside polar cap, nor does the leading edge of the patch on the dayside have to be the leading edge when the patch is on the nightside. This is especially the case for the given situation of a strong and varying IMF By component, when there is a substantial gradient across the polar cap in the antisunward flow speed.

[21] This data set may also offer opportunities to speculate on the source (ionization process and location) of the observed high-density plasma. However, persistent solar-EUV ionization is really the only way to generate the observed electron densities $n_e \geq 10^{12}$ m^{-3}. At the time (6 February 2001) more or less the entire Northern Hemisphere polar cap was in total darkness, so the extreme densities must have been produced elsewhere, i.e., at dayside sunlit lower latitudes, and transported into the high-latitude Svalbard region. We do not have any data to observe the actual production process, but the tracing in Figure 3 does suggest that the plasma came from lower latitudes. However, for event 1 there was poor SuperDARN coverage over mainland Scandinavia, so the backward tracing goes into a freeze around 0700 UT a few degrees of latitude south of Svalbard. For event 2 the backward tracing points at lower latitudes in the afternoon/evening sector as the most likely source location (i.e., over Russia), but there is also poor radar coverage in that area, so it remains a speculation. Still it should be pointed out that this hypothesis of the plasma coming from a lower-latitude reservoir in the afternoon sector is fully consistent with a large body of research literature in the field, including *Foster et al.* [2005].

3.2. Irregularity Generation

[22] The strong gradients in the plasma flow speed may in themselves also represent a potential generation mechanism for ionospheric irregularities, which SuperDARN obtains its radar echoes from. Presently there are two different mechanisms that are thought to dominate the generation of plasma irregularities at high latitudes and in the polar cap. The gradient drift instability occurs when there is plasma flow across a steep plasma density gradient [see, e.g., *Ossakow and Chaturvedi*, 1979; *Keskinen and Ossakow*, 1981, 1983; *Tsunoda*, 1988], and the velocity shear instability occurs when there are severe shears in the plasma flow [see, e.g., *Keskinen et al.*, 1988; *Basu et al.*, 1988, 1990; *Tsunoda*, 1988]. The gradient drift instability mechanism has long been regarded as the dominant mode for production of *F* region irregularities in the dayside cusp region [e.g., *Tsunoda*, 1988], but growth rate estimates based on observed plasma density gradients have shown that the gradient drift instability is too slow to explain observed irregularities alone [*Moen et al.*, 2000, 2002]. It is also supported by recent gradient drift modeling work [*Gondarenko and Guzdar*, 1999, 2004a, 2004b]. Recently, *Carlson et al.* [2007, 2008] suggested a new process for cusp irregularities, where both mechanisms (gradient drift and velocity-shear) work together in the plasma structuring process. Shear-driven instabilities rapidly structure the entering plasma, and gradient drift instabilities build on these large "seed" irregularities.

[23] Although the studies of *Carlson et al.* [2007, 2008] only focused on the dayside cusp region, we assume that this dual-mechanism process may also be in operation elsewhere, like across the entire polar cap. Given the strong flow shears that were observed (see Figures 2f, 3a, 3d, and 4) gradients in the plasma flow existed for an extended time. When a patch of extreme plasma density E × B-drifts in a nonuniform electric field, the associated flow shears may rotate, stretch, or squeeze the high-density patch. As can be seen from Figure 3, the patch was continuously changing its orientation for the nearly 2 h it took to cross the polar cap. Consequently, the velocity-shear mechanism may operate for considerably longer time periods than was originally proposed by *Carlson et al.* [2007, 2008], thereby giving the gradient drift instability even more "seed" irregularities to work with, at least for the IMF By conditions in our case where there are strong gradients in the plasma flow. The net result will be plasma irregularities that continue to grow at a high rate all the way across the polar cap. This may also be part of the reason why SuperDARN radars are so efficient at detecting echoes deep into the polar cap. As can be seen in Figure 4, the Kodiak backscatter power from event 2 (Figures 4e–4g) was quite significant, over 2 h after the patch left the dayside. However, more modeling work will be needed to understand the effects that these velocity gradients have on high-density patches.

3.3. Plasma Flow Variability

[24] Figure 3 revealed that the flow speed was pulsed when the high-density patch traversed the polar cap. Transient flow enhancements were seen both equatorward of the dayside cusp region (before the patch entered Svalbard), in the vicinity of the dayside cusp (over Svalbard), and across the polar cap. In the dayside cusp ionosphere there have been numerous reports of pulsed flows on newly opened magnetic field lines in response to transient reconnection on the dayside magnetopause [e.g., *Denig et al.*, 1993; *Lockwood et al.*, 1993, 2005a, 2005b; *Moen et al.*, 2001, 2008b; *Oksavik et al.*, 2004, 2005; *Rinne et al.*, 2007], and pulses of transient reconnection have been suggested as a dominating mechanism for polar cap patch formation [*Lockwood and Carlson*, 1992; *Carlson et al.*, 2004, 2006]. There have also been several reports of bursts or transients in the sunward return flow on closed magnetic field lines at lower latitudes in the morning and/or afternoon sectors [e.g., *Moen et al.*, 1995] and in the sunward flow of the Sub-Auroral Polarization Stream (SAPS) [e.g., *Foster et al.*, 2004; *Oksavik et al.*, 2006b].

[25] Recently, *Sandholt and Farrugia* [2009] reported the existence of a channel of enhanced antisunward flow on "old open field lines" (i.e., field lines that were opened >10 min

ago) at the dawn or dusk flanks of the polar cap. Some of their events were very similar, with IMF By > 0 and a narrow channel of enhanced antisunward flow in the dawn sector of the Northern Hemisphere polar cap, like the situation we have around 0800 UT in Figure 2g. *Lockwood et al.* [1990] state that momentum transfer is restricted only to "newly opened field lines," and *Cowley and Lockwood* [1992] argue that the flow in the polar cap is driven only by two intrinsically time-dependent components, dayside reconnection and nightside reconnection. The dayside reconnection voltage maximizes just poleward of the dayside open/closed boundary and falls off across the polar cap toward zero on the nightside, and the nightside reconnection voltage is strongest on the nightside and falls off toward the dayside. Consequently, the net flow in the central polar cap (i.e., local polar cap potential) is then driven by a sum of the two processes. *Sandholt and Farrugia* [2009] on the other hand, argue that when IMF is dominated by By there can also be significant momentum transfer also on "old open magnetic field lines" that are connected to dynamo action in the high-latitude boundary layer tailward of the cusp [*Cowley*, 1981; *Stern*, 1984; *Siscoe et al.*, 1991, 2000; *Taguchi et al.*, 1993]. The electric field from this momentum transfer maps to one of the flanks of the polar cap (the exact flank depends on the sign of IMF By), where it gives rise to an asymmetry in the flow and the observed channel of intense flow in the dawn or dusk flanks of the polar cap. *Sandholt and Farrugia* [2009] also found the flow channel to be associated with mantle and polar rain precipitation and for our situation here (Bx < 0, By > 0 and Northern Hemisphere) that the polar rain contains a "solar wind strahl" component. The "strahl" is the closely field-aligned electron component of the solar wind halo population that is observed to have direct access to the magnetospheric lobe in the hemisphere where particle entry is favored by the IMF Bx polarity, as documented by, e.g., *Fairfield and Scudder* [1985]. However, *Sandholt and Farrugia* [2009] based their study on drift meter data from individual DMSP satellite passes, and they were therefore unable to observe the pulsed nature of the flow that we see within this channel here (e.g., in Figure 3). We therefore think our study is also the first report of pulsed flow in this channel on "old open field lines."

[26] In Figure 5 we bring this discussion one step further. Figure 5a shows a dawn-dusk meridional cut across the polar cap (see Figure 2f), and we have indicated with dotted lines (in Figure 5) the convection reversal boundary in the dawn and dusk sectors. The width of the antisunward flow channel is shown with thick black lines, and for simplicity it is defined as the full width at half maximum (FWHM). In Figure 5b we compare the potentials in the dawn sector (dotted red), the dusk sector (dotted green), the entire total polar cap (dashed black), and the antisunward flow channel (solid blue). If we use the time interval 0700–0800 UT as an example, we notice three things: (1) consistent with IMF By > 0, the SuperDARN map potential model indicates a higher net potential in the dusk sector than in the dawn sector; (2) consistent with pulsed flow, the net potential in the antisunward flow channel is highly variable; and (3) a significant fraction of the total polar cap potential is from the intense channel of antisunward flow. In Figure 5c we compare each potential to the total polar cap potential. For the time range 0700–0900 UT we notice that 60–90% of the total polar cap potential is from the intense channel of antisunward flow.

[27] This finding is significant. It means that the momentum transfer process in the high-latitude boundary layer is not constant; it must be transient as well, just like for "newly open field lines" near the open/closed boundary on the dayside. It means that there must be pulsed momentum transfer when the field lines also connect to the high-latitude boundary layer, not just when the field lines are newly opened and connected to the low-latitude subsolar magnetopause. The *Cowley and Lockwood* [1992] model will in principle give pulsed flow in the polar cap, if either the dayside or nightside reconnection rates are pulsed. But it seems unlikely that this will result in pulsed flows that channeled in a narrow region (only a few hundred kilometers wide) that extends across the entire polar cap. How can this flow channel maintain its narrow shape over thousands of kilometers, if the only generators are located near the dayside and nightside open/closed boundaries? Either there must be a generator in the high-latitude boundary layer that continue to transfer momentum to the central polar cap long after the field lines have been opened on the dayside, or perhaps *Lockwood et al.* [1990] underestimated the duration of the momentum transfer process when they said that the momentum transfer is only active during the first few minutes (i.e., less than 10 min) after reconnection. This estimate is most likely true for a classical IMF Bz southward situation. But in the extreme situation when IMF By is large and dominating, the field lines at the flanks of the polar cap may be draped around the magnetosphere, even past the equator and to high latitudes in the other hemisphere. Once a new field line has been opened, it could undergo substantial zonal motion before it begins its antisunward motion. In the Northern Hemisphere, when IMF is dominated by IMF By positive, magnetic reconnection in the dayside postnoon sector will force a newly opened field line to move in the direction of the IMF from dusk toward dawn (i.e., the initial force is along the dusk-dawn line). On the other hand, the solar wind pull will be in the antisunward direction. When the reconnection rate is large, the field line may move a significant distance along the dusk-dawn line before the solar wind pull takes over and starts to pull the field line in the antisunward direction. It could therefore take significantly more than 10 min to completely straighten out the very long field line. Consequently, the field line may experience a significant pull far into the mantle and tail lobes. If this tensioning of the field line occurs in a pulsed manner (either due to pulsed reconnection or pulsed tension on the field line from the solar wind), it would result in pulsed flow in the ionosphere, even far into the polar cap.

[28] In Figure 6 we present a sketch which will attempt to illustrate how this may take place. In this analysis we have chosen to use event 2 because there was data from the Kodiak radar on the nightside to verify its path across the polar cap. The T96 model [*Tsyganenko*, 1995, 1996], with given activity level indexes (IMF, solar wind pressure, and Dst), has been used to draw the magnetic field lines. As the starting position we use the sequence of ionospheric MLAT-MLT coordinates that were obtained from our par-

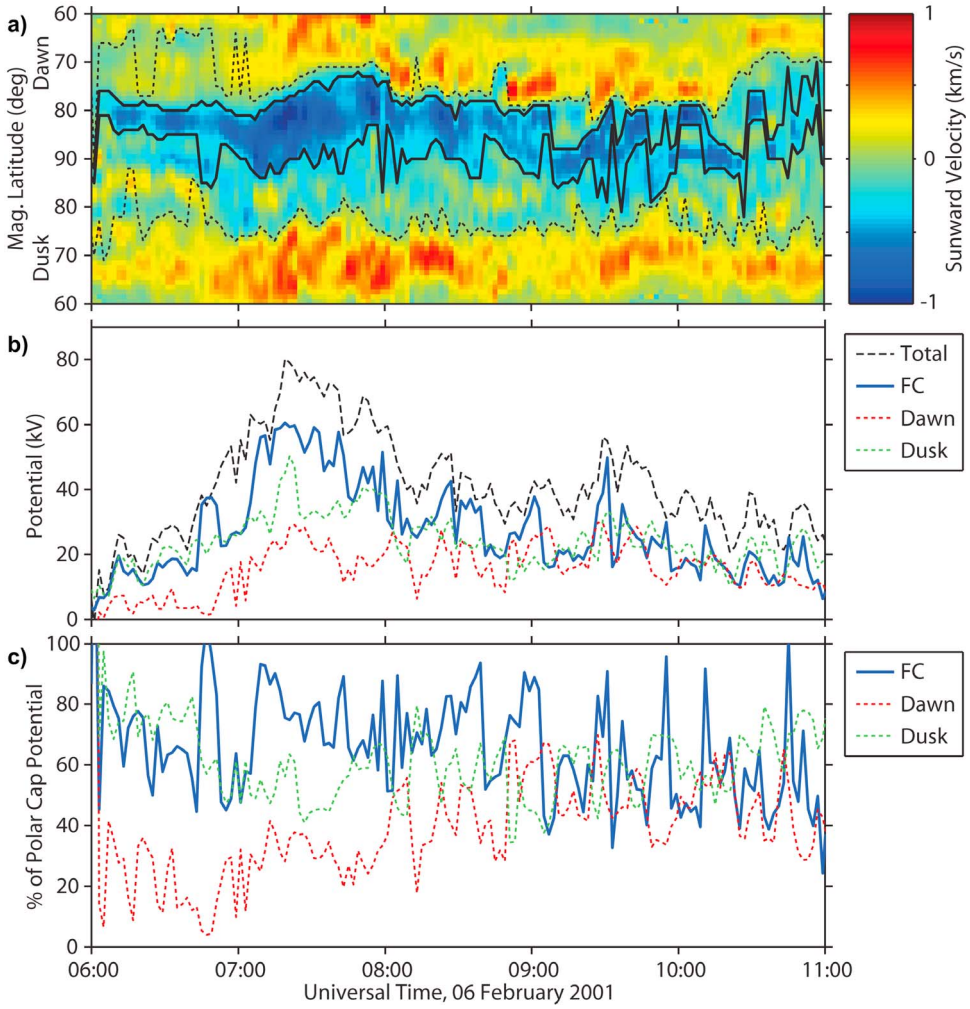

Figure 5. A quantitative summary of the absolute and relative contributions to the polar cap potential of the intense antisunward flow channel. (a) Sunward (in red colors) and antisunward (in blue colors) SuperDARN plasma flow in a dawn-dusk meridional cut across the polar cap at 0600 and 1800 MLT. Overlaid are the convection reversal boundaries (black dotted lines) and the width of the antisunward flow channel (black solid lines). (b) Net potentials in the dawn sector (dotted red), the dusk sector (dotted green), the entire total polar cap (dashed black), and the antisunward flow channel (solid blue). (c) A comparison of each potential to the total polar cap potential; i.e., how many percent of the total polar cap potential it is.

ticle tracing of event 2 in Figure 3, and the T96 model has been used to draw the corresponding magnetic field line every 4 min. In the next step all resulting field lines in the time range 0730–0830 UT were overlaid in the same diagram to give a schematic picture of how the topology of the magnetic field changed as the high-density plasma drifted across the polar cap. Figures 6a and 6b show the situation of the leading edge of the high-density plasma that passed over the ESR at 0800 UT, and Figures 6c and 6d are for the trailing edge passing over the ESR at 0818 UT. The model magnetosphere is shaded in gray. In Figures 6a and 6c the magnetosphere is viewed from the Sun; with north facing up and dusk to the right. In Figures 6b and 6d the magnetosphere is viewed from the high north, with noon facing down and dusk to the right. In Figures 6a–6c the dotted red line indicates the overall motion of the field line.

[29] Several interesting aspects can be illustrated with this schematic. Although the T96 model claims that the field lines of the leading and trailing edges of the extreme density went from closed to open near magnetic noon almost simultaneously (0738 versus 0742 UT), the key feature to notice is really the completely different paths that the two edges of the extreme density event are following. The leading edge (Figures 6a and 6b) starts out as a closed magnetic field line near magnetic noon at 0730 UT, appears to open around 0742 UT, and drifts poleward across the dawn polar cap. The curvature of this field line quickly disappears, and at 0830 UT the field line has reached far into the tail lobes. On the other hand, the trailing edge (Figures 6c and 6d) starts out on a closed field line in the dusk sector at 0730 UT, appears to open around 0738 UT, and follows a track along the perimeter of the entire dawn flank magne-

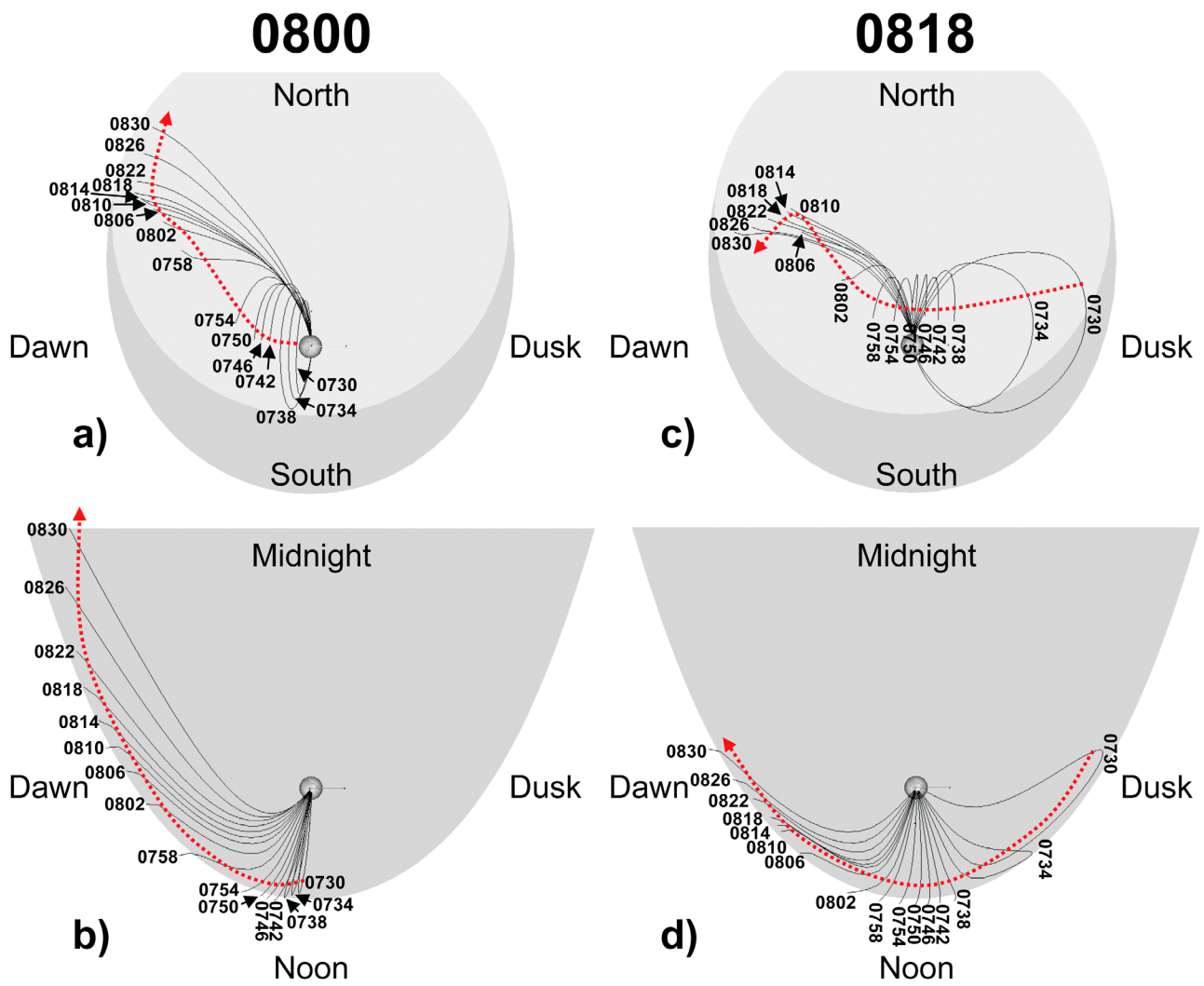

Figure 6. Resulting magnetic field line configurations based on a stepwise tracing of the ionospheric footprint of event 2 for the interval 0730–0830 UT. (a and b) The leading edge passing over the ESR at 0800 UT and (c and d) the trailing edge passing over the ESR at 0818 UT. The model magnetopause is shaded in gray. Please notice that darker color will appear where multiple surfaces are overlaid in the projection (like the nose and tail magnetopause in Figures 6a and 6c). Magnetic field lines are drawn every 4 min. In Figures 6a and 6c the magnetosphere is viewed from the Sun, with north facing up and dusk to the right. In Figures 6b and 6d the magnetosphere is viewed from the high north; with noon facing down and dusk to the right. In Figures 6a–6d the dotted red line indicates the overall motion of the field line. Please notice that the leading edge (Figures 6a and 6b) follows a completely different path than the trailing edge (Figures 6c and 6d).

tosphere. In 1 h the field line is pulled all the way from dusk to dawn along the entire dayside magnetopause. The pull and zonal motion is significant, and the field line remains curved for a much longer time than the 10 min proposed by *Lockwood et al.* [1990]. One can also notice that there is substantial twisting of the field line from 0810 to 0830 UT (see Figure 6c), when the field line maps to quite high latitudes (i.e., the mantle region). It should be emphasized that it is around this time when the Hankasalmi radar observed the severe rotation of the HF backscatter (see Figures 4a–4d). It should also be noted that the most severe rotation is taking place on the field line that is connected very close to the dawn flank. For the given By > 0 situation, field lines near the flank will have to traverse a longer distance along the dayside magnetopause, and the same field lines will therefore experience a significantly stronger pull from the solar wind. This example also documents how closely linked the dynamics of polar cap patches in the ionosphere is to the solar wind driver. We cannot discuss the dynamics of polar cap patches without also considering the propagation of magnetic field lines across the polar cap, i.e., the influence of the solar wind driver and the orientation of the IMF. The solar wind will have a direct influence on the dynamics of polar cap patches far into the polar cap. The momentum transfer may also be active several tens of minutes after the field line has been opened on the dayside, at least for the

given situation where IMF is dominated by a large By component.

4. Summary and Concluding Remarks

[30] In this paper we have used comprehensive observations from SuperDARN and the EISCAT Svalbard Radar to study two extreme density events ($n_e \geq 10^{12}$ m^{-3}) that drifted across the polar cap. Both events occurred in a period where IMF By was strongly positive, and they were first detected by the EISCAT Svalbard Radar on the dayside. Wide data coverage from SuperDARN was used to follow both events both forward and backward in time. Both events originated in the afternoon sector at lower sunlit latitudes, before the large-scale convection transported them into and across the polar cap. For the first event there was no data to verify the actual time of arrival on the nightside. The second event had extensive data coverage; the Hankasalmi radar confirmed how the event rotated in a clockwise direction once it entered the dayside polar cap, and the Kodiak radar verified the subsequent time of arrival on the nightside (i.e., confirming the accuracy of the tracing across the polar cap from Europe to Alaska). On its way across the polar cap the parcel of extreme density plasma experienced pulsed flow speed and substantial rotation.

[31] This study has several new findings: In the past, attention has mainly been on what happens to polar cap patches when they are created on the dayside near the open/closed field line boundary. Less attention has been devoted to their transit across the polar cap, implicitly assuming that they just follow the antisunward flow. The current study shows that this simplified picture must be advanced. Momentum transfer can last significantly longer than 10 min after reconnection, especially for extremely long field lines where IMF By is dominating, i.e., on "old open field lines." The flow speed across the polar cap can also be highly dynamic and pulsed. Patches can undergo substantial rotation in the central polar cap, so that the leading edge can become the trailing edge, and the first patch to enter the dayside polar cap may not be the first patch to reach the nightside. Plasma can be stagnant in the polar cap or even overtaken. The strong gradients in the plasma flow associated with the rotation may in itself also further enhance the growth of ionospheric irregularities all the way across the polar cap. With a quickly growing chain of new SuperDARN radars from midlatitudes to the central polar cap (e.g., StormDARN and PolarDARN) there will be unprecedented opportunities to further explore this phenomenon toward the upcoming solar maximum.

[32] **Acknowledgments.** We thank the ACE MAG instrument team and the ACE Science Center for providing the ACE data. Data from the SOHO and Wind spacecraft were provided by the Coordinated Data Analysis Web (CDA Web), and we thank the instrument teams for making the data available; SOHO CELIAS/MTOF Proton Monitor (PI: P. Bochsler), Wind Solar Wind Experiment (PI: K. Ogilvie), Wind Magnetic Fields Investigation (PI: R. Lepping), and Wind Three-Dimensional Plasma Analyzer (PI: R. Lin). EISCAT is an international association supported by research organizations in China (CRIRP), Finland (SA), France (CNRS, till end 2006), Germany (DFG), Japan (NIPR and STEL), Norway (NFR), Sweden (VR), and the United Kingdom (STFC). We thank the SuperDARN PIs for provision of the radar data. SuperDARN operations at the University of Leicester are supported by STFC grant PP/E007929/1, and ML is funded by STFC grants PP/E000983/1 and ST/H002480/1. This project has also been sponsored by the Research Council of Norway, the Air Force Office of Scientific Research, Air Force Material Command, USAF, under grant FA8655-10-1-3003, and COST action ES0803.

[33] Robert Lysak thanks the reviewers for their assistance in evaluating this paper.

References

Baker, K. B., R. A. Greenwald, J. M. Ruohoniemi, J. R. Dudeney, M. Pinnock, P. T. Newell, M. E. Greenspan, and C.-I. Meng (1990), Simultaneous HF-radar and DMSP observations of the cusp, *Geophys. Res. Lett.*, *17*(11), 1869–1872, doi:10.1029/GL017i011p01869.

Barth, V. L. (2009), Identification and tracking of extreme electron densities by EISCAT Svalbard radar and SuperDARN, Master thesis, Univ. of Oslo, Norway.

Basu, S., S. Basu, E. MacKenzie, P. F. Fougere, W. R. Coley, N. C. Maynard, J. D. Winningham, M. Sugiura, W. B. Hanson, and W. R. Hoegy (1988), Simultaneous density and electric field fluctuation spectra associated with velocity shears in the auroral oval, *J. Geophys. Res.*, *93*(A1), 115–136, doi:10.1029/JA093iA01p00115.

Basu, S., S. Basu, E. MacKenzie, W. R. Coley, J. R. Sharber, and W. R. Hoegy (1990), Plasma structuring by the gradient drift instability at high latitudes and comparison with velocity shear driven processes, *J. Geophys. Res.*, *95*(A6), 7799–7818, doi:10.1029/JA095iA06p07799.

Basu, S., E. J. Weber, T. W. Bullett, M. J. Keskinen, E. MacKenzie, P. Doherty, R. Sheehan, H. Kuenzler, P. Ning, and J. Bongiolatti (1998), Characteristics of plasma structuring in the cusp/cleft region at Svalbard, *Radio Sci.*, *33*(6), 1885–1899, doi:10.1029/98RS01597.

Basu, S., K. M. Groves, Su. Basu, and P. J. Sultan (2002), Specification and forecasting of scintillations in communication/navigation links: Current status and future plans, *J. Atmos. Sol. Terr. Phys.*, *64*(16), 1745–1754.

Buchau, J., B. W. Reinisch, E. J. Weber, and J. G. Moore (1983), Structure and dynamics of the winter polar cap F region, *Radio Sci.*, *18*(6), 995–1010, doi:10.1029/RS018i006p00995.

Buchau, J., E. J. Weber, D. N. Anderson, H. C. Carlson Jr., J. G. Moore, B. W. Reinisch, and R. C. Livingston (1985), Ionospheric structures in the polar cap: Their origin and relation to 250-MHz scintillation, *Radio Sci.*, *20*(3), 325–338, doi:10.1029/RS020i003p00325.

Bust, G. S., and G. Crowley (2007), Tracking of polar cap ionospheric patches using data assimilation, *J. Geophys. Res.*, *112*, A05307, doi:10.1029/2005JA011597.

Carlson, H. C., Jr., K. Oksavik, J. Moen, and T. Pedersen (2004), Ionospheric patch formation: Direct measurements of the origin of a polar cap patch, *Geophys. Res. Lett.*, *31*, L08806, doi:10.1029/2003GL018166.

Carlson, H. C., J. Moen, K. Oksavik, C. P. Nielsen, I. W. McCrea, T. R. Pedersen, and P. Gallop (2006), Direct observations of injection events of subauroral plasma into the polar cap, *Geophys. Res. Lett.*, *33*, L05103, doi:10.1029/2005GL025230.

Carlson, H. C., T. Pedersen, S. Basu, M. Keskinen, and J. Moen (2007), Case for a new process, not mechanism, for cusp irregularity production, *J. Geophys. Res.*, *112*, A11304, doi:10.1029/2007JA012384.

Carlson, H. C., K. Oksavik, and J. Moen (2008), On a new process for cusp irregularity production, *Ann. Geophys.*, *26*, 2871–2885, doi:10.5194/angeo-26-2871-2008.

Cowley, S. W. H. (1981), Magnetospheric and ionospheric flow and the interplanetary magnetic field, in *The Physical Basis of the Ionosphere in the Solar-Terrestrial System*, *AGARD Conf. Proc.*, vol. 295, pp. 1–14, NATO, Neuilly Sur-Seine, France.

Cowley, S. W. H., and M. Lockwood (1992), Excitation and decay of solar wind-driven flows in the magnetosphere-ionosphere system, *Ann. Geophys.*, *10*, 103–115.

Crowley, G. (1996), Critical review of ionospheric patches and blobs, in *Review of Radio Science 1993–1996*, edited by W. R. Stone, pp. 619–648, Oxford Sci. Publ., Oxford, U. K.

Crowley, G., A. J. Ridley, D. Deist, S. Wing, D. J. Knipp, B. A. Emery, J. Foster, R. Heelis, M. Hairston, and B. W. Reinisch (2000), Transformation of high-latitude ionospheric F region patches into blobs during the March 21, 1990, storm, *J. Geophys. Res.*, *105*(A3), 5215–5230, doi:10.1029/1999JA900357.

Dandekar, B. S. (2002), Solar cycle dependence of polar cap patch activity, *Radio Sci.*, *37*(1), 1013, doi:10.1029/2000RS002562.

Dandekar, B. S., and T. W. Bullett (1999), Morphology of polar cap patch activity, *Radio Sci.*, *34*(5), 1187–1205, doi:10.1029/1999RS900056.

Davies, J. A., M. Lester, S. E. Milan, and T. K. Yeoman (1999), A comparison of velocity measurements from the CUTLASS Finland radar and the EISCAT UHF system, *Ann. Geophys.*, *17*, 892–902, doi:10.1007/s00585-999-0892-9.

Denig, W. F., W. J. Burke, N. C. Maynard, F. J. Rich, B. Jacobsen, P. E. Sandholt, A. Egeland, S. Leontjev, and V. G. Vorobjev (1993), Ionospheric signatures of dayside magnetopause transients: A case study

using satellite and ground measurements, *J. Geophys. Res.*, *98*(A4), 5969–5980, doi:10.1029/92JA01541.

Drayton, R. A., A. V. Koustov, M. R. Hairston, and J.-P. Villain (2005), Comparison of DMSP cross-track ion drifts and SuperDARN line-of-sight velocities, *Ann. Geophys.*, *23*, 2479–2486, doi:10.5194/angeo-23-2479-2005.

Fairfield, D. H., and J. D. Scudder (1985), Polar rain: Solar coronal electrons in the Earth's magnetosphere, *J. Geophys. Res.*, *90*(A5), 4055–4068, doi:10.1029/JA090iA05p04055.

Foster, J. C. (1993), Storm time plasma transport at middle and high latitudes, *J. Geophys. Res.*, *98*(A2), 1675–1689, doi:10.1029/92JA02032.

Foster, J. C., and W. J. Burke (2002), SAPS: A new categorization for sub-auroral electric fields, *Eos Trans. AGU*, *83*(36), 393–394, doi:10.1029/2002EO000289.

Foster, J. C., and J. R. Doupnik (1984), Plasma convection in the vicinity of the dayside cleft, *J. Geophys. Res.*, *89*(A10), 9107–9113, doi:10.1029/JA089iA10p09107.

Foster, J. C., P. J. Erickson, F. D. Lind, and W. Rideout (2004), Millstone Hill coherent-scatter radar observations of electric field variability in the sub-auroral polarization stream, *Geophys. Res. Lett.*, *31*, L21803, doi:10.1029/2004GL021271.

Foster, J. C., et al. (2005), Multiradar observations of the polar tongue of ionization, *J. Geophys. Res.*, *110*, A09S31, doi:10.1029/2004JA010928.

Gillies, R. G., G. C. Hussey, G. J. Sofko, K. A. McWilliams, R. A. D. Fiori, P. Ponomarenko, and J.-P. St.-Maurice (2009), Improvement of SuperDARN velocity measurements by estimating the index of refraction in the scattering region using interferometry, *J. Geophys. Res.*, *114*, A07305, doi:10.1029/2008JA013967.

Gondarenko, N. A., and P. N. Guzdar (1999), Gradient drift instability in high latitude plasma patches: Ion inertial effects, *Geophys. Res. Lett.*, *26*(22), 3345–3348, doi:10.1029/1999GL003647.

Gondarenko, N. A., and P. N. Guzdar (2004a), Density and electric field fluctuations associated with the gradient drift instability in the high-latitude ionosphere, *Geophys. Res. Lett.*, *31*, L11802, doi:10.1029/2004GL019703.

Gondarenko, N. A., and P. N. Guzdar (2004b), Plasma patch structuring by the nonlinear evolution of the gradient drift instability in the high-latitude ionosphere, *J. Geophys. Res.*, *109*, A09301, doi:10.1029/2004JA010504.

Grant, I. F., J. W. MacDougall, J. M. Ruohoniemi, W. A. Bristow, G. J. Sofko, J. A. Koehler, D. Danskin, and D. André (1995), Comparison of plasma flow velocities determined by the ionosonde Doppler drift technique, SuperDARN radars, and patch motion, *Radio Sci.*, *30*(5), 1537–1549, doi:10.1029/95RS00831.

Hosokawa, K., K. Shiokawa, Y. Otsuka, A. Nakajima, T. Ogawa, and J. D. Kelly (2006), Estimating drift velocity of polar cap patches with all-sky airglow imager at Resolute Bay, Canada, *Geophys. Res. Lett.*, *33*, L15111, doi:10.1029/2006GL026916.

Hosokawa, K., K. Shiokawa, Y. Otsuka, T. Ogawa, J.-P. St-Maurice, G. J. Sofko, and D. A. Andre (2009a), Relationship between polar cap patches and field-aligned irregularities as observed with an all-sky airglow imager at Resolute Bay and the PolarDARN radar at Rankin Inlet, *J. Geophys. Res.*, *114*, A03306, doi:10.1029/2008JA013707.

Hosokawa, K., T. Tsugawa, K. Shiokawa, Y. Otsuka, T. Ogawa, and M. R. Hairston (2009b), Unusually elongated, bright airglow plume in the polar cap F region: Is it a tongue of ionization?, *Geophys. Res. Lett.*, *36*, L07103, doi:10.1029/2009GL037512.

Hosokawa, K., T. Kashimoto, S. Suzuki, K. Shiokawa, Y. Otsuka, and T. Ogawa (2009c), Motion of polar cap patches: A statistical study with all-sky airglow imager at Resolute Bay, Canada, *J. Geophys. Res.*, *114*, A04318, doi:10.1029/2008JA014020.

Keskinen, M. J., and S. L. Ossakow (1981), On the spatial power spectrum of the E × B gradient drift instability in ionospheric plasma clouds, *J. Geophys. Res.*, *86*(A8), 6947–6950, doi:10.1029/JA086iA08p06947.

Keskinen, M. J., and S. L. Ossakow (1983), Theories of high-latitude ionospheric irregularities: A review, *Radio Sci.*, *18*(6), 1077–1091, doi:10.1029/RS018i006p01077.

Keskinen, M. J., H. G. Mitchell, J. A. Fedder, P. Satyanarayana, S. T. Zalesak, and J. D. Huba (1988), Nonlinear evolution of the Kelvin-Helmholtz instability in the high-latitude ionosphere, *J. Geophys. Res.*, *93*(A1), 137–152, doi:10.1029/JA093iA01p00137.

Knudsen, W. C. (1974), Magnetospheric convection and the high-latitude F2 ionosphere, *J. Geophys. Res.*, *79*(7), 1046–1055, doi:10.1029/JA079i007p01046.

Lockwood, M., and H. C. Carlson Jr. (1992), Production of polar cap electron density patches by transient magnetopause reconnection, *Geophys. Res. Lett.*, *19*(17), 1731–1734, doi:10.1029/92GL01993.

Lockwood, M., P. E. Sandholt, S. W. H. Cowley, and T. Oguti (1989), Interplanetary magnetic field control of dayside auroral activity and the transfer of momentum across the dayside magnetopause, *Planet. Space Sci.*, *37*(11), 1347–1365, doi:10.1016/0032-0633(89)90106-2.

Lockwood, M., S. W. H. Cowley, and M. P. Freeman (1990), The excitation of plasma convection in the high-latitude ionosphere, *J. Geophys. Res.*, *95*(A6), 7961–7972, doi:10.1029/JA095iA06p07961.

Lockwood, M., J. Moen, S. W. H. Cowley, A. D. Farmer, U. P. Løvhaug, H. Lühr, and V. N. Davda (1993), Variability of dayside convection and motions of the cusp/cleft aurora, *Geophys. Res. Lett.*, *20*(11), 1011–1014, doi:10.1029/93GL00846.

Lockwood, M., J. Moen, A. P. van Eyken, J. A. Davies, K. Oksavik, and I. W. McCrea (2005a), Motion of the dayside polar cap boundary during substorm cycles: I. Observations of pulses in the magnetopause reconnection rate, *Ann. Geophys.*, *23*, 3495–3511, doi:10.5194/angeo-23-3495-2005.

Lockwood, M., J. A. Davies, J. Moen, A. P. van Eyken, K. Oksavik, I. W. McCrea, and M. Lester (2005b), Motion of the dayside polar cap boundary during substorm cycles: II. Generation of poleward-moving events and polar cap patches by pulses in the magnetopause reconnection rate, *Ann. Geophys.*, *23*, 3513–3532, doi:10.5194/angeo-23-3513-2005.

Lorentzen, D. A., N. Shumilov, and J. Moen (2004), Drifting airglow patches in relation to tail reconnection, *Geophys. Res. Lett.*, *31*, L02806, doi:10.1029/2003GL017785.

McEwen, D. J., and D. P. Harris (1995), Observations of F layer patches and their convection over the north magnetic pole, *Adv. Space Res.*, *16*(1), 69–72, doi:10.1016/0273-1177(95)00101-J.

McEwen, D. J., and D. P. Harris (1996), Occurrence patterns of F layer patches over the north magnetic pole, *Radio Sci.*, *31*(3), 619–628, doi:10.1029/96RS00312.

McEwen, D. J., D. P. Harris, J. W. MacDougall, and I. F. Grant (1995), Drifting F-layer patches over the magnetic pole, *J. Geomagn. Geoelectr.*, *47*, 527–537.

McEwen, D. J., W. Guo, J. W. MacDougall, and P. T. Jayachandran (2004), The polar ionosphere, *Adv. Space Res.*, *34*(9), 2080–2084, doi:10.1016/j.asr.2004.06.011.

Milan, S. E., M. Lester, and T. K. Yeoman (2002), HF radar polar patch formation revisited: Summer and winter variations in dayside plasma structuring, *Ann. Geophys.*, *20*, 487–499, doi:10.5194/angeo-20-487-2002.

Milan, S. E., S. Basu, T. K. Yeoman, and R. E. Sheehan (2005), A comparison of satellite scintillation measurements with HF radar backscatter characteristics, *Ann. Geophys.*, *23*, 3451–3455, doi:10.5194/angeo-23-3451-2005.

Moen, J., P. E. Sandholt, M. Lockwood, W. F. Denig, U. P. Løvhaug, B. Lybekk, A. Egeland, D. Opsvik, and E. Friis-Christensen (1995), Events of enhanced convection and related dayside auroral activity, *J. Geophys. Res.*, *100*(A12), 23,917–23,934, doi:10.1029/95JA02585.

Moen, J., H. C. Carlson, S. E. Milan, N. Shumilov, B. Lybekk, P. E. Sandholt, and M. Lester (2000), On the collocation between dayside auroral activity and coherent HF radar backscatter, *Ann. Geophys.*, *18*, 1531–1549, doi:10.1007/s00585-001-1531-2.

Moen, J., A. P. van Eyken, and H. C. Carlson (2001), EISCAT Svalbard Radar observations of ionospheric plasma dynamics in relation to dayside auroral transients, *J. Geophys. Res.*, *106*(A10), 21,453–21,461, doi:10.1029/2000JA000378.

Moen, J., I. K. Walker, L. Kersley, and S. E. Milan (2002), On the generation of cusp HF backscatter irregularities, *J. Geophys. Res.*, *107*(A4), 1044, doi:10.1029/2001JA000111.

Moen, J., K. Oksavik, and H. C. Carlson (2004), On the relationship between ion upflow events and cusp auroral transients, *Geophys. Res. Lett.*, *31*, L11808, doi:10.1029/2004GL020129.

Moen, J., H. C. Carlson, K. Oksavik, C. P. Nielsen, S. E. Pryse, H. R. Middleton, I. W. McCrea, and P. Gallop (2006), EISCAT observations of plasma patches at sub-auroral cusp latitudes, *Ann. Geophys.*, *24*, 2363–2374, doi:10.5194/angeo-24-2363-2006.

Moen, J., N. Gulbrandsen, D. A. Lorentzen, and H. C. Carlson (2007), On the MLT distribution of F region polar cap patches at night, *Geophys. Res. Lett.*, *34*, L14113, doi:10.1029/2007GL029632.

Moen, J., X. C. Qiu, H. C. Carlson, R. Fujii, and I. W. McCrea (2008a), On the diurnal variability in F2-region plasma density above the EISCAT Svalbard radar, *Ann. Geophys.*, *26*, 2427–2433, doi:10.5194/angeo-26-2427-2008.

Moen, J., Y. Rinne, H. C. Carlson, K. Oksavik, R. Fujii, and H. Opgenoorth (2008b), On the relationship between thin Birkeland current arcs and reversed flow channels in the winter cusp/cleft ionosphere, *J. Geophys. Res.*, *113*, A09220, doi:10.1029/2008JA013061.

Ogawa, Y., S. C. Buchert, R. Fujii, S. Nozawa, and A. P. van Eyken (2009), Characteristics of ion upflow and downflow observed with the European Incoherent Scatter Svalbard radar, *J. Geophys. Res.*, *114*, A05305, doi:10.1029/2008JA013817.

Oksavik, K., J. Moen, and H. C. Carlson (2004), High-resolution observations of the small-scale flow pattern associated with a poleward moving

auroral form in the cusp, *Geophys. Res. Lett.*, *31*, L11807, doi:10.1029/2004GL019838.

Oksavik, K., J. Moen, H. C. Carlson, R. A. Greenwald, S. E. Milan, M. Lester, W. F. Denig, and R. J. Barnes (2005), Multi-instrument mapping of the small-scale flow dynamics related to a cusp auroral transient, *Ann. Geophys.*, *23*, 2657–2670, doi:10.5194/angeo-23-2657-2005.

Oksavik, K., J. M. Ruohoniemi, R. A. Greenwald, J. B. H. Baker, J. Moen, H. C. Carlson, T. K. Yeoman, and M. Lester (2006a), Observations of isolated polar cap patches by the European Incoherent Scatter (EISCAT) Svalbard and Super Dual Auroral Radar Network (SuperDARN) Finland radars, *J. Geophys. Res.*, *111*, A05310, doi:10.1029/2005JA011400.

Oksavik, K., R. A. Greenwald, J. M. Ruohoniemi, M. R. Hairston, L. J. Paxton, J. B. H. Baker, J. W. Gjerloev, and R. J. Barnes (2006b), First observations of the temporal/spatial variation of the sub-auroral polarization stream from the SuperDARN Wallops HF radar, *Geophys. Res. Lett.*, *33*, L12104, doi:10.1029/2006GL026256.

Ossakow, S. L., and P. K. Chaturvedi (1979), Current convective instability in the diffuse aurora, *Geophys. Res. Lett.*, *6*(4), 332–334, doi:10.1029/GL006i004p00332.

Pryse, S. E. (2003), Radio tomography: A new experimental technique, *Surv. Geophys.*, *24*, 1–38, doi:10.1023/A:1022272607747.

Pryse, S. E., A. G. Wood, H. R. Middleton, I. W. McCrea, and M. Lester (2006), Reconfiguration of polar-cap plasma in the magnetic midnight sector, *Ann. Geophys.*, *24*, 2201–2208, doi:10.5194/angeo-24-2201-2006.

Rinne, Y., J. Moen, K. Oksavik, and H. C. Carlson (2007), Reversed flow events in the winter cusp ionosphere observed by the European Incoherent Scatter (EISCAT) Svalbard radar, *J. Geophys. Res.*, *112*, A10313, doi:10.1029/2007JA012366.

Rodger, A. S., and A. C. Graham (1996), Diurnal and seasonal occurrence of polar cap patches, *Ann. Geophys.*, *14*, 533–537, doi:10.1007/s00585-996-0533-5.

Rodger, A. S., M. Pinnock, J. R. Dudeney, K. B. Baker, and R. A. Greenwald (1994a), A new mechanism for polar patch formation, *J. Geophys. Res.*, *99*(A4), 6425–6436, doi:10.1029/93JA01501.

Rodger, A. S., M. Pinnock, J. R. Dudeney, J. Waterman, O. de la Beaujardiere, and K. B. Baker (1994b), Simultaneous two hemisphere observations of the presence of polar patches in the nightside ionosphere, *Ann. Geophys.*, *12*, 642–648, doi:10.1007/s00585-994-0642-y.

Ruohoniemi, J. M., and K. B. Baker (1998), Large-scale imaging of high-latitude convection with Super Dual Auroral Radar Network HF radar observations, *J. Geophys. Res.*, *103*(A9), 20,797–20,811, doi:10.1029/98JA01288.

Ruohoniemi, J. M., and R. A. Greenwald (1996), Statistical patterns of high-latitude convection obtained from Goose Bay HF radar observations, *J. Geophys. Res.*, *101*(A10), 21,743–21,763, doi:10.1029/96JA01584.

Ruohoniemi, J. M., R. A. Greenwald, K. B. Baker, J. P. Villain, and M. A. McCready (1987), Drift motions of small-scale irregularities in the high-latitude F region: An experimental comparison with plasma drift motions, *J. Geophys. Res.*, *92*(A5), 4553–4564, doi:10.1029/JA092iA05p04553.

Sandholt, P. E., and C. J. Farrugia (2009), Plasma flow channels at the dawn/dusk polar cap boundaries: Momentum transfer on old open field lines and the roles of IMF By and conductivity gradients, *Ann. Geophys.*, *27*, 1527–1554, doi:10.5194/angeo-27-1527-2009.

Sato, T. (1959), Morphology of Ionospheric F2 disturbances in the polar region, *Rep. Ionos. Space Res. Jpn.*, *13*, 91–104.

Schunk, R. W., and J. J. Sojka (1996), Ionosphere-thermosphere space weather issues, *J. Atmos. Terr. Phys.*, *58*(14), 1527–1574, doi:10.1016/0021-9169(96)00029-3.

Siscoe, G., W. Lotko, and B. Sonnerup (1991), A high–latitude, low–latitude boundary layer model of the convection current system, *J. Geophys. Res.*, *96*(A3), 3487–3495, doi:10.1029/90JA02362.

Siscoe, G. L., G. M. Erickson, B. U. Ö. Sonnerup, N. C. Maynard, K. D. Siebert, D. R. Weimer, and W. W. White (2000), Deflected magnetosheath flow at the high-latitude magnetopause, *J. Geophys. Res.*, *105*(A6), 12,851–12,857, doi:10.1029/1999JA000268.

Stern, D. P. (1984), Magnetospheric dynamo processes, in *Magnetospheric Currents*, *Geophys. Monogr. Ser.*, vol. 28, edited by T. A. Potemra, pp. 200–207, AGU, Washington, D.C.

Taguchi, S., M. Sugiura, J. D. Winningham, and J. A. Slavin (1993), Characterization of the IMF By-dependent field-aligned currents in the cleft region based on DE 2 observations, *J. Geophys. Res.*, *98*(A2), 1393–1407, doi:10.1029/92JA01014.

Tsunoda, R. T. (1988), High-latitude F region irregularities: A review and synthesis, *Rev. Geophys.*, *26*(4), 719–760, doi:10.1029/RG026i004p00719.

Tsyganenko, N. A. (1995), Modeling the Earth's magnetospheric magnetic field confined within a realistic magnetopause, *J. Geophys. Res.*, *100*(A4), 5599–5612, doi:10.1029/94JA03193.

Tsyganenko, N. A. (1996), Effects of the solar wind conditions on the global magnetospheric configuration as deduced from data-based field models, *Eur. Space Agency Spec. Publ.*, *389*, 181–185.

Valladares, C. E., S. Basu, J. Buchau, and E. Friis-Christensen (1994), Experimental evidence for the formation and entry of patches into the polar cap, *Radio Sci.*, *29*(1), 167–194, doi:10.1029/93RS01579.

Valladares, C. E., D. T. Decker, R. Sheehan, and D. N. Anderson (1996), Modeling the formation of polar cap patches using large plasma flows, *Radio Sci.*, *31*(3), 573–593, doi:10.1029/96RS00481.

Villain, J. P., G. Caudal, and C. Hanuise (1985), A Safari-Eiscat comparison between the velocity of F region small-scale irregularities and the ion drift, *J. Geophys. Res.*, *90*(A9), 8433–8443, doi:10.1029/JA090iA09p08433.

Walker, I. K., J. Moen, L. Kersley, and D. A. Lorentzen (1999), On the possible role of cusp/cleft precipitation in the formation of polar-cap patches, *Ann. Geophys.*, *17*, 1298–1305, doi:10.1007/s00585-999-1298-4.

Weber, E. J., J. Buchau, J. G. Moore, J. R. Sharber, R. C. Livingston, J. D. Winningham, and B. W. Reinisch (1984), F layer ionization patches in the polar cap, *J. Geophys. Res.*, *89*(A3), 1683–1694, doi:10.1029/JA089iA03p01683.

Wood, A. G., S. E. Pryse, H. R. Middleton, and V. S. C. Howells (2008), Multi-instrument observations of nightside plasma patches under conditions of IMF Bz positive, *Ann. Geophys.*, *26*, 2203–2216, doi:10.5194/angeo-26-2203-2008.

Wood, A. G., S. E. Pryse, and J. Moen (2009), Modulation of nightside polar patches by substorm activity, *Ann. Geophys.*, *27*, 3923–3932, doi:10.5194/angeo-27-3923-2009.

Xu, L., A. V. Koustov, J. Thayer, and M. A. McCready (2001), SuperDARN convection and Sondrestrom plasma drift, *Ann. Geophys.*, *19*, 749–759, doi:10.5194/angeo-19-749-2001.

Yeh, H.-C., J. C. Foster, F. J. Rich, and W. Swider (1991), Storm time electric field penetration observed at midlatitude, *J. Geophys. Res.*, *96*(A4), 5707–5721, doi:10.1029/90JA02751.

Yeoman, T. K., D. M. Wright, A. J. Stocker, and T. B. Jones (2001), An evaluation of range accuracy in the Super Dual Auroral Radar Network over-the-horizon HF radar systems, *Radio Sci.*, *36*(4), 801–813, doi:10.1029/2000RS002558.

V. L. Barth, J. Moen, and K. Oksavik, University Centre in Svalbard, P.B. 156, NO-9171 Longyearbyen, Norway. (kjellmar.oksavik@unis.no)

M. Lester, Department of Physics and Astronomy, University of Leicester, Leicester LE1 7RH, UK.